



Article

# Adsorption Performance of Amino Functionalized Magnetic Molecular Sieve Adsorbent for Effective Removal of Lead Ion from Aqueous Solution

Chuanen Guo <sup>1</sup>, Yingying Wang <sup>2</sup>, Fangzheng Wang <sup>2</sup> and Yaoguang Wang <sup>2,\*</sup> <sup>1</sup> Shandong University of Political Science and Law, Jinan 250014, China; 000807@sdupsl.edu.cn<sup>2</sup> Shandong Provincial Key Laboratory of Molecular Engineering, School of Chemistry and Chemical Engineering, Qilu University of Technology (Shandong Academy of Sciences), Jinan 250353, China; yingyingw1203@163.com (Y.W.); wangfzhyx@163.com (F.W.)

\* Correspondence: wangyaoguang@qlu.edu.cn

**Abstract:** Lead ion (Pb<sup>2+</sup>) has high toxicity and brings great harm to human body. It is very important to find an effective method to address lead ion pollution. In this work, amino functionalized CoFe<sub>2</sub>O<sub>4</sub>/SBA-15 nanocomposite (NH<sub>2</sub>-CoFe<sub>2</sub>O<sub>4</sub>/SBA-15) was prepared for the effective removal of Pb<sup>2+</sup> from aqueous solution. The prepared NH<sub>2</sub>-CoFe<sub>2</sub>O<sub>4</sub>/SBA-15 adsorbent was manifested by using scanning electron microscope (SEM), energy dispersive spectroscopy (EDS), Fourier transform infrared spectrum (FTIR), X-ray powder diffraction (XRD), and Brunauer-Emmett-Teller (BET) analysis. In the meantime, the adsorption conditions, including pH, adsorbent dosage, and adsorption time, were studied. The investigation of adsorption kinetics revealed that the adsorption results conform to the pseudo-first-order kinetic model. The adsorption isotherms research displayed that the adsorption was consistent with the Freundlich model, demonstrating that the adsorption for Pb<sup>2+</sup> with the prepared adsorbent was a multimolecular layer adsorption process. In addition, the thermodynamic investigations ( $\Delta G < 0$ ,  $\Delta H > 0$ ,  $\Delta S > 0$ ) demonstrated that the adsorption for Pb<sup>2+</sup> with the prepared adsorbent was endothermic and spontaneous. Moreover, the prepared adsorbent showed superior anti-interference performance and reusability, implying the potential application of the adsorbent in actual water treatment. Furthermore, this research may provide a reference and basis for the study of other heavy metal ions.

**Keywords:** adsorption; amino functionalized CoFe<sub>2</sub>O<sub>4</sub>; SBA-15; magnetic separation; lead ion



**Citation:** Guo, C.; Wang, Y.; Wang, F.; Wang, Y. Adsorption Performance of Amino Functionalized Magnetic Molecular Sieve Adsorbent for Effective Removal of Lead Ion from Aqueous Solution. *Nanomaterials* **2021**, *11*, 2353. <https://doi.org/10.3390/nano11092353>

Academic Editor: Francesco Enrichi

Received: 14 August 2021

Accepted: 8 September 2021

Published: 11 September 2021

**Publisher's Note:** MDPI stays neutral with regard to jurisdictional claims in published maps and institutional affiliations.



**Copyright:** © 2021 by the authors. Licensee MDPI, Basel, Switzerland. This article is an open access article distributed under the terms and conditions of the Creative Commons Attribution (CC BY) license (<https://creativecommons.org/licenses/by/4.0/>).

## 1. Introduction

In the process of industrial production, the substandard discharge of wastewater releases a variety of heavy metal ions into the natural environment. A great quantity of heavy metal ions become one of the main environmental pollutants [1,2]. These dissolved heavy metal ions in water can cause adverse effects on aquatic ecosystems. Long-term exposure to water which has been contaminated by heavy metals can cause serious harm to human health [3–6]. Lead ion (Pb<sup>2+</sup>) is a common pollutant in industrial wastewater, which can cause human dysfunction or serious lesions if ingested in large quantities or for a long time [7,8]. For example, Pb<sup>2+</sup> can cause liver and kidney damage, affect the production of human hemoglobin, damage the human nervous system, cause mental retardation in infants, cause infertility and fetal malformation, etc. [9]. The general techniques for the removal of heavy metal ions in water include precipitation [10], ion exchange [11], reverse osmosis [12], nanofiltration [13], adsorption [14], etc. Among them, the adsorption method has gained extensive attention due to its simple, low cost and can overcome some potential environmental problems [15–18].

Since adsorbents with large specific surface area have a strong adsorption capacity, many researches with regard to adsorbents have focused on materials with a large specific

surface area [19–22]. A molecular sieve is a kind of material with large surface area. Moreover, it also possesses the advantages of stable physical and chemical properties, uniform pore size distribution, and easy to achieve chemical modification, etc. [23–26]. Therefore, a molecular sieve is a kind of adsorbing material with great potential. SBA-15 is a typical molecular sieve with a uniform mesoporous structure [27,28]. The mesoporous pore provides enough space for chemical modification of grafted functional groups, while sufficient wall thickness makes it exhibit superior mechanical stability and hydrothermal stability than similar materials [29,30]. These above properties provide reliable guarantee for designing adsorbents. The development of mesoporous silica adsorbents functionalized with appropriate functional groups is a prospective research area for eliminating heavy metal ions away from water resources [31,32].

For the purpose of improving the magnetic solid-liquid separation efficiency toward the adsorbent [33,34], we prepared the magnetic molecular sieve adsorbent by compositing SBA-15 and magnetic  $\text{CoFe}_2\text{O}_4$ , which could be separated well from water through an external magnetic field. To improve the adsorption capacity of the adsorbent, the surface of the prepared  $\text{CoFe}_2\text{O}_4/\text{SBA-15}$  nanocomposite was aminated to enhance the complexation ability toward heavy metal ions. Herein, the adsorption properties of amino functionalized  $\text{CoFe}_2\text{O}_4/\text{SBA-15}$  nanocomposite ( $\text{NH}_2\text{-CoFe}_2\text{O}_4/\text{SBA-15}$ ) for  $\text{Pb}^{2+}$  were investigated by using single factor experiment to optimize the adsorption process (Figure 1). Meanwhile, the adsorption kinetics, adsorption isotherm model and thermodynamic studies were investigated. Moreover, the prepared  $\text{NH}_2\text{-CoFe}_2\text{O}_4/\text{SBA-15}$  adsorbent exhibited excellent selectivity and reusability for adsorbing  $\text{Pb}^{2+}$ , indicating the potential application of the adsorbent in the field of environmental protection.



**Figure 1.** The schematic diagram for the application of  $\text{NH}_2\text{-CoFe}_2\text{O}_4/\text{SBA-15}$  toward  $\text{Pb}^{2+}$  adsorption in the presence of external magnetic field.

## 2. Experimental Section

### 2.1. Apparatus and Reagents

SBA-15 (CAS Number: 12173-28-3, pore diameter: 6–11 nm) was obtained from XFNANO Materials Tech Co., Ltd. (Nanjing, China).  $\text{Fe}(\text{NO}_3)_3$  was purchased from Sinopharm Chemical Reagent Beijing Co., Ltd. (Beijing, China).  $\text{Co}(\text{NO}_3)_2 \cdot 6\text{H}_2\text{O}$  was obtained from Macklin Biochemical Co., Ltd. (Shanghai, China). 3-aminopropyltriethoxysilane was purchased from Aladdin Bio-Chem Technology Co., Ltd. (Shanghai, China). Ultrapure

water was applied in all experiment for the preparation of solution. All other reagents were employed with analytical reagent grade and used without further purification.

Scanning electron microscope (SEM) pictures were conducted with field-emission SEM (Gemini 300, Zeiss, Jena, Germany). Fourier transform infrared spectrum (FTIR) spectra was obtained by using KBr pellet method ranging from  $4000\text{ cm}^{-1}$  to  $400\text{ cm}^{-1}$  with Perkin–Elmer Spectrum One FTIR spectrometer (Perkin–Elmer, Waltham, MA, USA). X-ray powder diffraction (XRD) pattern was obtained by using a D8 FOCUS X–ray diffraction spectrometer (Bruker, Karlsruhe, Germany), together with a Cu  $K\alpha$  target at a scanning rate of  $0.03^\circ\ 2\theta\ \text{s}^{-1}$  in the range of  $10\text{--}80^\circ$ . Brunauer-Emmett-Teller (BET) analysis was conducted by using Micromeritics ASAP 2020 surface area and porosity analyzer (Quantachrome, Boynton Beach, FL, USA). The atomic absorption spectrophotometry was proceeded by using an atomic absorption spectrophotometer (Perkin-Elmer, Waltham, MA, USA).

### 2.2. Synthesis of Magnetic $\text{CoFe}_2\text{O}_4/\text{SBA-15}$

$\text{CoFe}_2\text{O}_4/\text{SBA-15}$  was synthesized by one step immersion method as follows: Firstly, 0.116 g of  $\text{Co}(\text{NO}_3)_2\cdot 6\text{H}_2\text{O}$  and 0.323 g of  $\text{Fe}(\text{NO}_3)_3$  were mixed in three-neck flask with 20 mL of ultrapure water. Then 0.2 g of SBA-15 was added into the above solution with stir for mixing well. Afterwards, the flask was moved to the oil bath under  $50^\circ\text{C}$  with continuous agitation. After the water in flask been evaporated to dryness, the obtained solid was moved to crucible and calcined for 5 h at  $800^\circ\text{C}$ . Eventually, the magnetic  $\text{CoFe}_2\text{O}_4/\text{SBA-15}$  could be obtained.

### 2.3. Synthesis of Amino Functionalized $\text{CoFe}_2\text{O}_4/\text{SBA-15}$

0.5 g of  $\text{CoFe}_2\text{O}_4/\text{SBA-15}$  was dispersed into 50 mL of absolute ethanol. Then 1 mL of 3-aminopropyltriethoxysilane (APTES) was injected into the solution, followed with mechanically stirring and maintaining in oil bath for 24 h. The obtained solid was separated under magnetic field and rinsed with ethanol several times. After being disposed in drying oven at  $60^\circ\text{C}$ , the product was grinded and the  $\text{NH}_2\text{-CoFe}_2\text{O}_4/\text{SBA-15}$  could be obtained.

### 2.4. Single Factor Static Adsorption Experiment

This research was conducted by using single factor static adsorption method for investigating the adsorption of  $\text{Pb}^{2+}$  onto  $\text{NH}_2\text{-CoFe}_2\text{O}_4/\text{SBA-15}$ . The adsorption experiment was proceeded in 100 mL of conical flask at ambient temperature by placing the conical flask in a thermostatic water bath oscillator, along with  $\text{Pb}^{2+}$  solution ( $30\text{ mg}\cdot\text{L}^{-1}$ , 25 mL).  $0.1\text{ mol}\cdot\text{L}^{-1}$  of  $\text{NaNO}_3$  was injected into the  $\text{Pb}^{2+}$  solution as constant back–ground electrolyte. The effect of adsorbent dosage for adsorbing  $\text{Pb}^{2+}$  was operated by using different amounts of adsorbent contacting with  $\text{Pb}^{2+}$  for 3 h. The pH was adjusted by using HCl and NaOH for studying the influence of pH toward the adsorption of  $\text{Pb}^{2+}$ . The adsorbent could be separated rapidly from solution by a magnet. The residual  $\text{Pb}^{2+}$  concentration in equilibrium was monitored by using atomic absorption spectrophotometry. Furthermore, the interfering ion experiment and the reusability of the prepared adsorbent were also investigated.

The removal efficiency as well as the adsorbing capacity were calculated based on the changes of  $\text{Pb}^{2+}$  concentration before and after the adsorption on the basis of the following calculation method:

$$R = \frac{c_0 - c_e}{c_0} \times 100\% \quad (1)$$

$$q_e = \frac{(c_0 - c_e) \times V}{m} \quad (2)$$

where  $c_0$  ( $\text{mg}\cdot\text{L}^{-1}$ ) and  $c_e$  ( $\text{mg}\cdot\text{L}^{-1}$ ) represent the initial and equalized contents of  $\text{Pb}^{2+}$ , respectively.  $R$  (%) is the removal efficiency and  $q_e$  ( $\text{mg}\cdot\text{g}^{-1}$ ) is the adsorption capacity when the adsorption becomes equilibrium. The volume of  $\text{Pb}^{2+}$  solution is expressed as  $V$  (L) and the mass of adsorbent is described as  $m$  (g).

### 3. Results and Discussion

#### 3.1. Characterization of $\text{NH}_2\text{-CoFe}_2\text{O}_4/\text{SBA-15}$

Figure 2A,B show the morphology of SBA-15 and  $\text{CoFe}_2\text{O}_4/\text{SBA-15}$ . As can be seen from Figure 2A, the SBA-15 owned chaplet-like shape. Observed from Figure 2B, the surface of SBA-15 appeared new nanoparticles, which was due to the formation of  $\text{CoFe}_2\text{O}_4$ . Furthermore, energy dispersive spectroscopy (EDS) was applied to analysis the component of the adsorbent. As Figure 2C shows, the adsorbent contained not only the elements of Si and O, but also contained Fe and Co, demonstrating the existence of constituent elements for  $\text{CoFe}_2\text{O}_4/\text{SBA-15}$ .

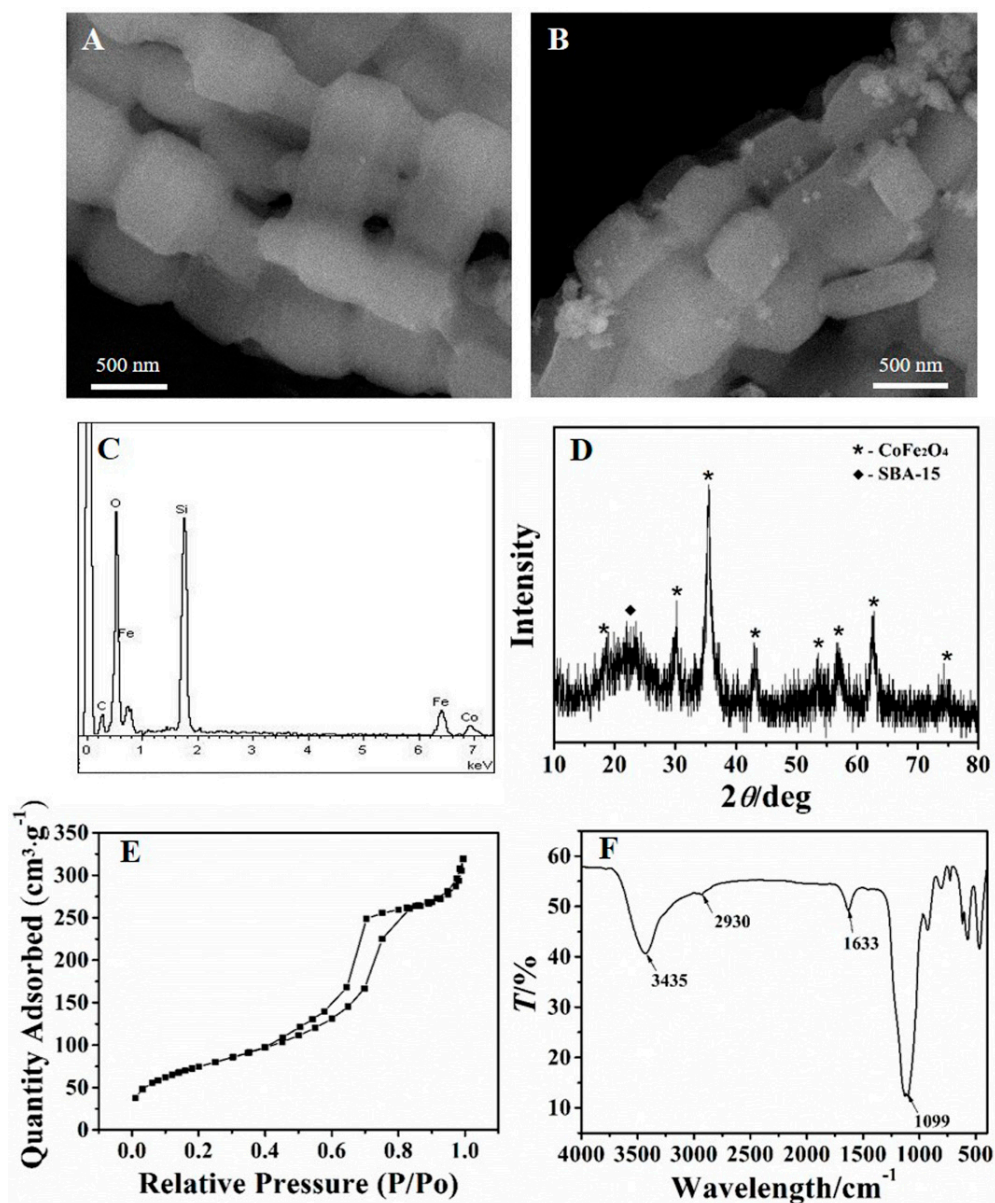


Figure 2. SEM images of SBA-15 (A) and  $\text{CoFe}_2\text{O}_4/\text{SBA-15}$  (B); EDS spectrum of  $\text{CoFe}_2\text{O}_4/\text{SBA-15}$  (C); XRD pattern (D), BET analysis (E), and FTIR spectrum (F) of  $\text{NH}_2\text{-CoFe}_2\text{O}_4/\text{SBA-15}$ .

The XRD pattern was further used to analysis the  $\text{NH}_2\text{-CoFe}_2\text{O}_4/\text{SBA-15}$ . As shown in Figure 2D, the dispersion peak nearly  $2\theta = 23^\circ$  was attributed to the amorphous SBA-15. The other diffraction peaks in the figure were consistent with the spectrum of  $\text{CoFe}_2\text{O}_4$  [35]. According to the above results, it could conclude that the  $\text{CoFe}_2\text{O}_4$  was loaded on SBA-15 successfully.

Figure 2E shows the BET analysis of  $\text{NH}_2\text{-CoFe}_2\text{O}_4/\text{SBA-15}$ . Since the existence of the adsorption and desorption hysteresis loop, it is obvious that the  $\text{NH}_2\text{-CoFe}_2\text{O}_4/\text{SBA-15}$  owns uniform and orderly mesoporous channels, which is beneficial for adsorbing  $\text{Pb}^{2+}$ . The specific surface area which was measured for the prepared  $\text{NH}_2\text{-CoFe}_2\text{O}_4/\text{SBA-15}$  was about  $273.8 \text{ m}^2\cdot\text{g}^{-1}$ , which was lower than pure SBA-15 (about  $550 \text{ m}^2\cdot\text{g}^{-1}$ ). This might be due to the fact that the introduction of  $\text{CoFe}_2\text{O}_4$  blocked the pores of SBA-15, and thus the specific surface area of  $\text{NH}_2\text{-CoFe}_2\text{O}_4/\text{SBA-15}$  decreased.

Figure 2F displays the FTIR spectrum of  $\text{NH}_2\text{-CoFe}_2\text{O}_4/\text{SBA-15}$ . As shown in the spectrum, the bond of N–H stretching vibration can be testified by the peak at  $3435 \text{ cm}^{-1}$ , while the peak at the position of  $1633 \text{ cm}^{-1}$  belonged to the deformation vibration absorption peak of N–H. The peaks at  $2930 \text{ cm}^{-1}$  were the absorption peak of C–H. The peak at  $1099 \text{ cm}^{-1}$  was the Si–O absorption peak of SBA-15. The results further illustrated the successful synthesis of  $\text{NH}_2\text{-CoFe}_2\text{O}_4/\text{SBA-15}$ .

### 3.2. Influence of pH toward Removal Efficiency

The pH of the employed solution is considered to be a critical ingredient to impact the adsorption process [36]. The impact is mainly reflected in the following aspects. Firstly, the solution pH could affect the charge type and charge number on the adsorbent, which determines whether the adsorption process can either occur or not occur. Secondly, the charge number on the adsorbent surface determines the molar ratio of adsorbent and adsorbate when it reaches saturated adsorption. Thirdly, the pH could influence the existing form of pollutant, further affect the state of adsorbent or pollutant, which determines the mechanism of the adsorption process.

In this study, we mainly investigated the effect of pH toward the adsorption of  $\text{Pb}^{2+}$  with  $\text{NH}_2\text{-CoFe}_2\text{O}_4/\text{SBA-15}$ . The experiment was conducted as follows: 25 mL  $30 \text{ mg}\cdot\text{L}^{-1}$  of  $\text{Pb}^{2+}$  solution was added into the 100 mL conical flask.  $\text{HNO}_3$  and  $\text{NaOH}$  were applied to adjust the pH. Then 10 mg of adsorbent was added and vibrated for 3 h at room temperature. The residual  $\text{Pb}^{2+}$  was measured and the removal efficiency could be obtained. Observed from Figure 3A, when the pH of the solution was under 4.0, the efficiency for the removal of  $\text{Pb}^{2+}$  was very low. With the increase of the pH, the removal efficiency increased. And the maximum removal efficiency was from pH 5.0 to pH 6.0. This result could be interpreted as follows: When at low pH, the  $\text{H}^+$  and  $\text{Pb}^{2+}$  in solution were competitive with each other. And the  $\text{H}^+$  could protonate the  $-\text{NH}_2$  on the surface of adsorbent. The surface of the adsorbent is positively charged, which could repel with  $\text{Pb}^{2+}$  because of the static electricity. Furthermore, the  $\text{H}^+$  hindered the coordination between  $\text{Pb}^{2+}$  and adsorbent, decreasing the adsorption capacity of the adsorbent. However, when the pH increased, the  $-\text{NH}_2$  on the surface of adsorbent deprotonated. Then the  $-\text{NH}_2$  as electron-rich group would attract a positively charged  $\text{Pb}^{2+}$  and complex with it. Thus, the adsorption capacity increased. According to the experimental results, the optimal pH 5.0 was chosen for future experiment.

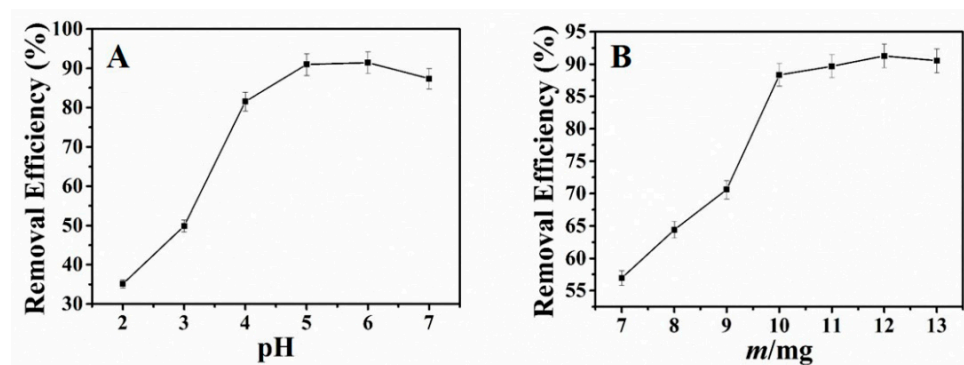


Figure 3. Effect of pH (A) and adsorbent dosage (B) on adsorption of  $\text{Pb}^{2+}$  (initial content of  $\text{Pb}^{2+}$ :  $25 \text{ mL } 30 \text{ mg}\cdot\text{L}^{-1}$ ; time: 3 h; temperature: ambient temperature).

### 3.3. Effect of Adsorbent Dosage on the Removal Efficiency

Selected amount of  $\text{NH}_2\text{-CoFe}_2\text{O}_4/\text{SBA-15}$  were added into 100 mL round-bottom flask with 25 mL  $30\text{ mg}\cdot\text{L}^{-1}$  of  $\text{Pb}^{2+}$  (pH 5.0) and agitated for 3 h at ambient temperature. The influence of adsorbent dosage toward the removal of  $\text{Pb}^{2+}$  displays in Figure 3B. When the adsorbent dosage aggrandized, the removal efficiency for  $\text{Pb}^{2+}$  fortified. As the adsorbent dosage was 10 mg, the removal efficiency became very high and changed little with the increase of the adsorbent dosage. Thus, the adsorbent dosage of 10 mg was selected in the subsequent experiment.

### 3.4. Influence of Adsorption Time and Adsorption Kinetics

Adsorption kinetics resulting from the adsorption process are crucial in the process of studying adsorption behavior, which reflects the basic information of adsorption rate and reaction routes [37,38]. The effect of adsorption time was investigated in this study. In the condition of the selected pH and adsorbent dosage in the preliminary experiment, different adsorption times were applied to investigate the adsorption of  $\text{Pb}^{2+}$  by using  $\text{NH}_2\text{-CoFe}_2\text{O}_4/\text{SBA-15}$ . As shown in Figure 4A, the adsorption process reached equilibrium at 150 min.

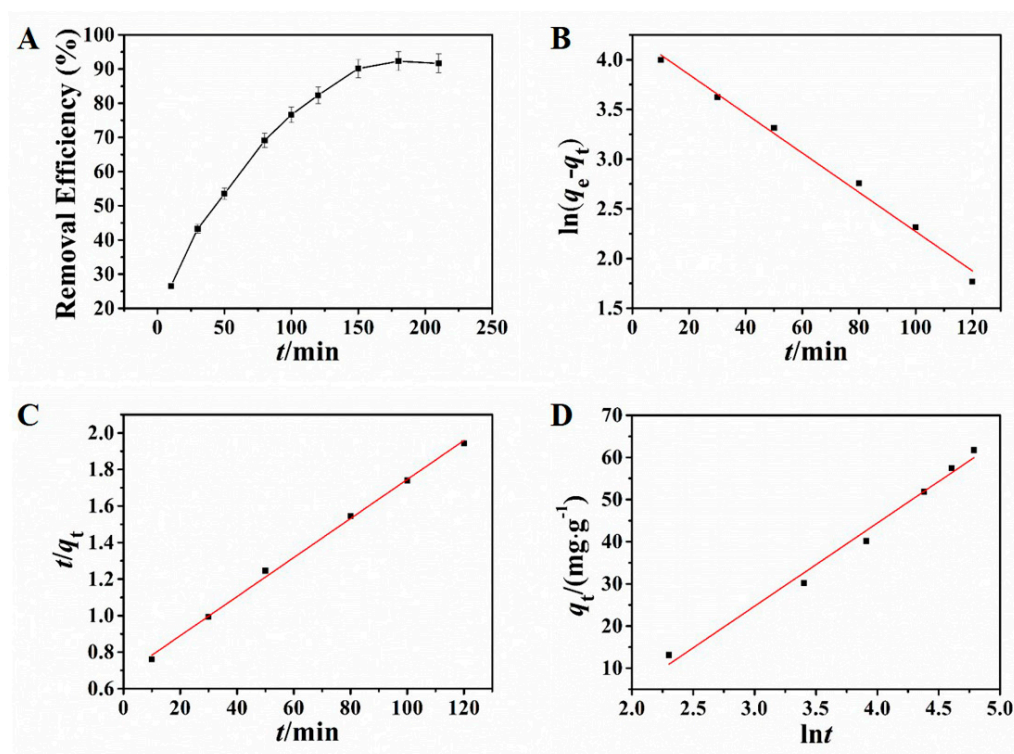


**Figure 4.** Influence of adsorption time toward the removal efficiency (A); pseudo-first-order kinetic model (B), pseudo-second-order kinetic model (C), and Elovich kinetic model (D) for adsorption of  $\text{Pb}^{2+}$ .

Adsorption kinetics has been an important aspect for study the adsorption mechanism. Herein, the pseudo-first-order kinetic model, pseudo-second-order kinetic model, and Elovich kinetic model were employed to explore the dynamics features for the adsorption behavior. Each model could be presented below:

Pseudo-first-order kinetic model:

$$\ln(q_e - q_t) = \ln q_e - k_1 t \quad (3)$$

Pseudo-second-order kinetic model:

$$\frac{t}{q_t} = \frac{1}{k_2 q_e^2} + \frac{t}{q_e} \quad (4)$$

Elovich kinetic model:

$$q_t = \frac{1}{\beta} \ln(\alpha \cdot \beta) + \frac{1}{\beta} \ln(t/\text{min}) \quad (5)$$

here  $q_t$  ( $\text{mg}\cdot\text{g}^{-1}$ ) represents the adsorption capacities at time  $t$  (min).  $q_e$  ( $\text{mg}\cdot\text{g}^{-1}$ ) represents the adsorption capacities at equilibrium adsorption. The pseudo-first-order rate constant and pseudo-second-order rate constant are denoted as  $k_1$  ( $\text{min}^{-1}$ ) and  $k_2$  ( $\text{g}\cdot\text{mg}^{-1}\cdot\text{min}^{-1}$ ) separately. The initial adsorption rate in Elovich model is defined as  $\alpha$  ( $\text{mg}\cdot\text{g}^{-1}\cdot\text{min}^{-1}$ ), while the desorption constant is expressed as  $\beta$  ( $\text{g}\cdot\text{mg}^{-1}$ ).

The kinetic results are displayed in Figure 4B–D and the corresponding calculative results were presented in Table 1. Observed from the matching results, either the pseudo-first-order kinetic model or the pseudo-second-order kinetic model had high linear coefficient. However, the test result of the equilibrium adsorbing amount was  $67.61 \text{ mg}\cdot\text{g}^{-1}$ , close to the result from the pseudo-first-order kinetic model ( $69.78 \text{ mg}\cdot\text{g}^{-1}$ ). The relative error was only 3.2%, indicating that the adsorption kinetic process can be fitted splendidly by pseudo-first-order kinetic model, indicating that the adsorption behavior was dominated by diffusion step.

**Table 1.** Kinetic model parameters for the adsorption of  $\text{Pb}^{2+}$ .

Models	Parameters	
Pseudo-first-order kinetic model	$q_e$ ( $\text{mg}\cdot\text{g}^{-1}$ )	69.78
	$k_1$ ( $\text{min}^{-1}$ )	0.01974
	$R^2$	0.9898
Pseudo-second-order kinetic model	$q_e$ ( $\text{mg}\cdot\text{g}^{-1}$ )	94.34
	$k_2$ ( $\text{g}\cdot\text{mg}^{-1}\cdot\text{min}^{-1}$ )	0.0001660
	$R^2$	0.9974
Elovich kinetic model	$\alpha$ ( $\text{mg}\cdot\text{g}^{-1}\cdot\text{min}^{-1}$ )	3.436
	$\beta$ ( $\text{g}\cdot\text{mg}^{-1}$ )	0.05071
	$R^2$	0.9842

### 3.5. Adsorption Isotherms Study

Herein, four kinds of adsorption isotherm models were applied to investigate the surface behavior of the prepared adsorbent in the solution:

Henry model:

$$q_e = k c_e \quad (6)$$

Langmuir model:

$$\frac{1}{q_e} = \frac{1}{b q_m c_e} + \frac{1}{q_m} \quad (7)$$

Freundlich model:

$$\ln q_e = \ln K_F + \frac{1}{n} \ln c_e \quad (8)$$

Temkin model:

$$q_e = \frac{RT}{b_T} \ln c_e + \frac{RT}{b_T} \ln A_T \quad (9)$$

where  $q_m$  ( $\text{mg}\cdot\text{g}^{-1}$ ) represents the maximum adsorption capacity.  $b$  ( $\text{L}\cdot\text{mg}^{-1}$ ) represents Langmuir constant about the binding capacity of the binding site.  $k$  ( $\text{L}\cdot\text{g}^{-1}$ ) and  $K_F$  ( $\text{L}\cdot\text{g}^{-1}$ ) represent the corresponding constants for adsorption capacity and strength.  $\frac{RT}{b_T}$  is relevant toward the adsorption heat.  $A_T$  ( $\text{L}\cdot\text{g}^{-1}$ ) represents the constant in equilibrium related with

the supreme binding energy.  $n$  (dimensionless) is an empirical parameter related to the intensity of adsorption, which varies with the heterogeneity of the adsorbent.

Figure 5 revealed the results of adsorption isotherms which were fitted by the above four models. The parameters which were calculated according to the four models are presented in Table 2. Observed from Table 2, the adsorption behavior could be well fitted by using the Freundlich model ( $R^2 = 0.9942$ ) which is higher than the correlation coefficient of other models. The simulated results revealed that the adsorption behavior was consistent with the Freundlich model, manifesting that the adsorption for  $Pb^{2+}$  was a multi-molecular layer adsorption process.

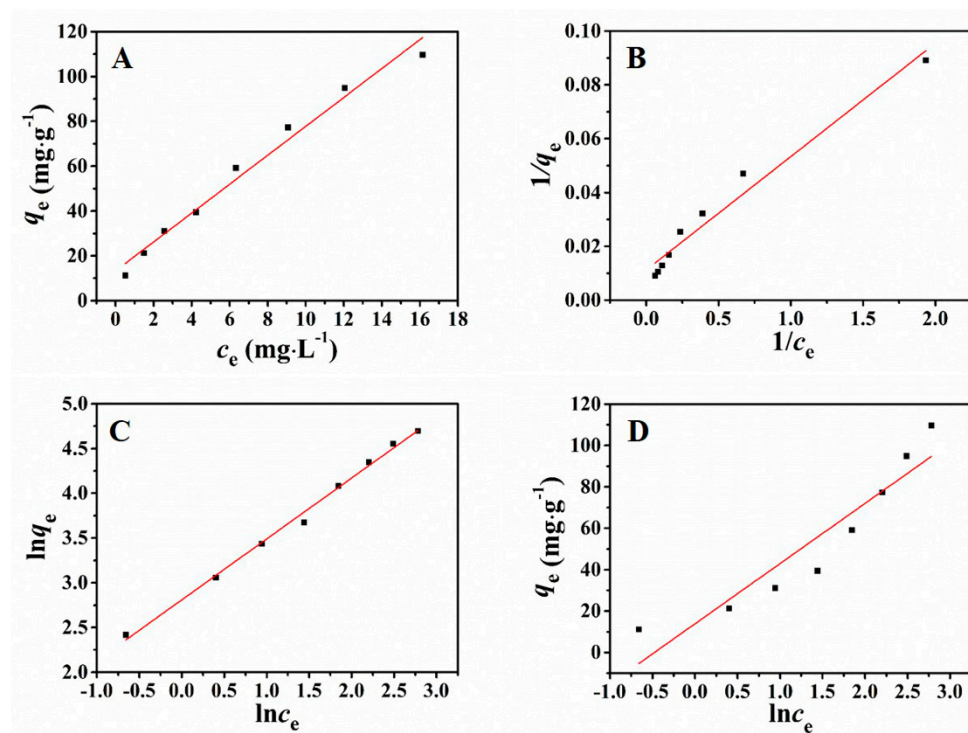


Figure 5. Henry (A), Langmuir (B), Freundlich (C), and Temkin (D) adsorption isotherms of  $Pb^{2+}$ .

Table 2. Parameters of adsorption isotherm for adsorbing  $Pb^{2+}$  with  $NH_2-CoFe_2O_4/SBA-15$ .

Models	Parameters	
Henry	$k$	6.447
	$R^2$	0.9782
Langmuir	$q_m$ ( $mg \cdot g^{-1}$ )	89.13
	$b$ ( $L \cdot mg^{-1}$ )	0.2664
	$R^2$	0.9641
Freundlich	$K_F$	16.71
	$n$	1.470
	$R^2$	0.9942
Temkin	$b_T$	88.0
	$A_T$	1.613
	$R^2$	0.8659

The Freundlich isotherm model demonstrates that the ratio of solute adsorbed on solid surface to the solute concentration has a certain relationship toward the solution concentration. This model considers multiple types of adsorption sites on the solid and represents the adsorption data at low concentrations and intermediate concentrations on

heterogeneous surfaces felicitously. And the symbol of  $n$  reveals that the adsorption process occurs on the heterogeneous surfaces and is a reversible course.

### 3.6. Thermodynamic Parameters Study

The influence of temperatures on  $\text{Pb}^{2+}$  adsorption was investigated under the temperatures of 298 K, 308 K, and 318 K. The thermodynamic variables were obtained by using the calculation method below:

$$\Delta G = -RT \ln K_d \quad (10)$$

$$\ln K_d = \frac{\Delta S}{R} - \frac{\Delta H}{RT} \quad (11)$$

Herein,  $R$  ( $8.314 \text{ J}\cdot\text{mol}^{-1}\cdot\text{K}^{-1}$ ) represents the gas constant.  $T$  represents the (Kelvin) temperature ( $K$ ).  $K_d$  represents the adsorption equilibrium constant. The Gibbs free energy change is defined as  $\Delta G$  ( $\text{kJ}\cdot\text{mol}^{-1}$ ). The entropy change is expressed as  $\Delta S$  ( $\text{J}\cdot\text{mol}^{-1}\cdot\text{K}^{-1}$ ). Furthermore,  $\Delta H$  ( $\text{kJ}\cdot\text{mol}^{-1}$ ) demonstrates the enthalpy change in a given process. The obtained results of the thermodynamic parameters were displayed in Table 3. From the table, it can be seen that the  $\Delta G$  was less than 0, indicating the spontaneous adsorption process for the removal of  $\text{Pb}^{2+}$ . While the  $\Delta H$  with positive value manifested the endothermic process of the adsorption for  $\text{Pb}^{2+}$  by using the prepared adsorbent. Meanwhile, the positive value of  $\Delta S$  indicated the increase in degree of chaos at the interface of solid and solution as well as the good affinity of  $\text{Pb}^{2+}$  with  $\text{NH}_2\text{-CoFe}_2\text{O}_4/\text{SBA-15}$ .

**Table 3.** Thermodynamic parameters for adsorption of  $\text{Pb}^{2+}$  with  $\text{NH}_2\text{-CoFe}_2\text{O}_4/\text{SBA-15}$ .

$T$ (K)	$\Delta G$ ( $\text{kJ}\cdot\text{mol}^{-1}$ )	$\Delta S$ ( $\text{J}\cdot\text{mol}^{-1}\cdot\text{K}^{-1}$ )	$\Delta H$ ( $\text{kJ}\cdot\text{mol}^{-1}$ )
298	−5.45		
308	−6.66	121.5	30.76
318	−7.88		

### 3.7. Evaluation of Adsorption Performance

The existing interfering ions including  $\text{Na}^+$ ,  $\text{K}^+$ ,  $\text{Mg}^{2+}$  and  $\text{Ca}^{2+}$  might influence the adsorption of  $\text{Pb}^{2+}$ . Hence the adsorption interference experiments were conducted by adding  $\text{NaNO}_3$ ,  $\text{KNO}_3$ ,  $\text{Mg}(\text{NO}_3)_2$  and  $\text{Ca}(\text{NO}_3)_2$  into the solutions containing lead ions, respectively. Observed from Figure 6A, the concomitant interfering ions almost had no influence on the  $\text{Pb}^{2+}$  adsorption. Therefore, it could be concluded that the prepared adsorbent can adsorb  $\text{Pb}^{2+}$  effectively.

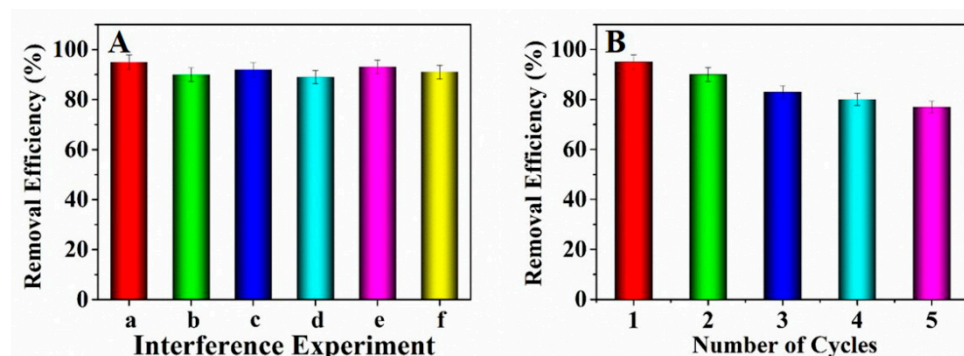


**Figure 6.** (A) Influence of interfering ions for  $\text{Pb}^{2+}$  adsorption (a: blank; b:  $\text{Na}^+$ ; c:  $\text{K}^+$ ; d:  $\text{Mg}^{2+}$ ; e:  $\text{Ca}^{2+}$ ; f: mixture of the above ions); (B) Reusability about the prepared adsorbent.

The reusability is an important index to investigate the property of the adsorbent [39]. Herein, to investigate the reusability of the prepared adsorbent, an adsorption-desorption experiment was conducted by adding the adsorbent which has adsorbed  $\text{Pb}^{2+}$  into 15 mL of  $\text{NaOH}$  solution ( $0.1 \text{ mol}\cdot\text{L}^{-1}$ ) and maintained for 3 h. Afterwards, the adsorbent

was washed with ultrapure water to remove the excess alkali solution for three times. Observed from Figure 6B, five times of adsorption-desorption cycles were studied. The consequences showed that the adsorption efficiency decreased to some extent. After five cycles, the removal efficiency kept at above 77%, indicating that the prepared adsorbent  $\text{NH}_2\text{-CoFe}_2\text{O}_4/\text{SBA-15}$  possessed good performance as recyclable adsorbent in dealing with the wastewater containing  $\text{Pb}^{2+}$ .

#### 4. Conclusions

In conclusion, a novel  $\text{NH}_2\text{-CoFe}_2\text{O}_4/\text{SBA-15}$  adsorbent was prepared and applied in the adsorption of  $\text{Pb}^{2+}$ . The adsorption results revealed that the adsorption behavior intensively relied on the pH of the solution with an adsorbent dosage of 10 mg and pH 5.0. The results of adsorption kinetics research can be well described by the pseudo-first-order kinetic model, revealing that the adsorption process was controlled by diffusion step. Meanwhile, the adsorption isotherms research indicated that the adsorption behavior could be expressed better through the Freundlich model. The thermodynamic studies ( $\Delta G < 0$ ,  $\Delta H > 0$ ,  $\Delta S > 0$ ) revealed the endothermic and spontaneous character of the adsorption behavior. The excellent selectivity and reusability of the prepared adsorbent made it a promising adsorbing material in the treatment of actual wastewater containing lead ions. However, the prepared adsorbent could only adsorb the single  $\text{Pb}^{2+}$ . If the adsorbent could interact with other contaminants simultaneously and effectively, it will greatly expand its application in the field of environmental protection.

**Author Contributions:** Conceptualization, Y.W. (Yaoguang Wang); methodology, C.G. and Y.W. (Yingying Wang); validation, Y.W. (Yaoguang Wang); formal analysis, C.G. and F.W.; investigation, C.G. and Y.W. (Yingying Wang); resources, Y.W. (Yaoguang Wang); data curation, C.G. and Y.W. (Yaoguang Wang); writing—original draft preparation, C.G. and Y.W. (Yingying Wang); writing—review and editing, Y.W. (Yaoguang Wang); visualization, Y.W. (Yaoguang Wang); supervision, Y.W. (Yaoguang Wang); project administration, Y.W. (Yaoguang Wang); funding acquisition, Y.W. (Yaoguang Wang). All authors have read and agreed to the published version of the manuscript.

**Funding:** This study was supported by the National Natural Science Foundation of China (22006080), Shandong Provincial Natural Science Foundation (ZR2020QB094), the Program for Scientific Research Innovation Team in Colleges and Universities of Shandong Province.

**Data Availability Statement:** The data presented in this study are available on request from the corresponding author.

**Conflicts of Interest:** The authors declare no conflict of interest.

#### References

1. Peng, Y.; Huang, H.; Zhang, Y.; Kang, C.; Chen, S.; Song, L.; Liu, D.; Zhong, C. A versatile MOF-based trap for heavy metal ion capture and dispersion. *Nat. Commun.* **2018**, *9*, 187. [[CrossRef](#)] [[PubMed](#)]
2. Sarma, D.; Islam, S.M.; Subrahmanyam, K.S.; Kanatzidis, M.G. Efficient and selective heavy metal sequestration from water by using layered sulfide  $\text{K}_{2x}\text{Sn}_{4-x}\text{S}_{8-x}$  ( $x = 0.65 - 1$ ; KTS-3). *J. Mater. Chem. A* **2016**, *4*, 16597–16605. [[CrossRef](#)]
3. Mao, M.; Yan, T.; Shen, J.; Zhang, J.; Zhang, D. Selective capacitive removal of heavy metal ions from wastewater over lewis base sites of S-Doped Fe-N-C cathodes via an electro-adsorption process. *Environ. Sci. Technol.* **2021**, *55*, 7665–7673. [[CrossRef](#)] [[PubMed](#)]
4. Mao, M.; Yan, T.; Shen, J.; Zhang, J.; Zhang, D. Capacitive removal of heavy metal ions from wastewater via an electro-adsorption and electro-reaction coupling process. *Environ. Sci. Technol.* **2021**, *55*, 3333–3340. [[CrossRef](#)] [[PubMed](#)]
5. Wei, Y.; Zhao, Y.; Zhao, X.; Gao, X.; Zheng, Y.; Zuo, H.; Wei, Z. Roles of different humin and heavy-metal resistant bacteria from composting on heavy metal removal. *Bioresour. Technol.* **2020**, *296*, 122375. [[CrossRef](#)]
6. Wang, Y.; Wang, Y.; Wang, F.; Chi, H.; Zhao, G.; Zhang, Y.; Li, T.; Wei, Q. Electrochemical aptasensor based on gold modified thiol graphene as sensing platform and gold-palladium modified zirconium metal-organic frameworks nanozyme as signal enhancer for ultrasensitive detection of mercury ions. *J. Colloid Interface Sci.* **2021**, *606*, 510–517. [[CrossRef](#)] [[PubMed](#)]
7. Zhang, L.; Shang, Z.; Guo, K.; Chang, Z.; Liu, H.; Li, D. Speciation analysis and speciation transformation of heavy metal ions in passivation process with thiol-functionalized nano-silica. *Chem. Eng. J.* **2019**, *369*, 979–987. [[CrossRef](#)]
8. He, Q.; Han, Y.; Huang, Y.; Gao, J.; Gao, Y.; Han, L.; Zhang, Y. Reusable dual-enhancement SERS sensor based on graphene and hybrid nanostructures for ultrasensitive lead (II) detection. *Sens. Actuators B Chem.* **2021**, *341*, 130031. [[CrossRef](#)]

9. Wang, Y.; Zhao, G.; Zhang, G.; Zhang, Y.; Wang, H.; Cao, W.; Li, T.; Wei, Q. An electrochemical aptasensor based on gold -modified MoS<sub>2</sub>/rGO nanocomposite and gold -palladium -modified Fe-MOFs for sensitive detection of lead ions. *Sens. Actuators B Chem.* **2020**, *319*, 128313. [[CrossRef](#)]
10. Grimshaw, P.; Calo, J.M.; Hradil, G. Cyclic electrowinning/precipitation (CEP) system for the removal of heavy metal mixtures from aqueous solutions. *Chem. Eng. J.* **2011**, *175*, 103–109. [[CrossRef](#)]
11. Bashir, A.; Malik, L.A.; Ahad, S.; Manzoor, T.; Bhat, M.A.; Dar, G.N.; Pandith, A.H. Removal of heavy metal ions from aqueous system by ion-exchange and biosorption methods. *Environ. Chem. Lett.* **2019**, *17*, 729–754. [[CrossRef](#)]
12. Malamis, S.; Katsou, E.; Takopoulos, K.; Demetriou, P.; Loizidou, M. Assessment of metal removal, biomass activity and RO concentrate treatment in an MBR-RO system. *J. Hazard. Mater.* **2012**, *209*, 1–8. [[CrossRef](#)]
13. Balanya, T.; Labanda, J.; Llorens, J.; Sabate, J. Separation of metal ions and chelating agents by nanofiltration. *J. Membr. Sci.* **2009**, *345*, 31–35. [[CrossRef](#)]
14. Wang, Y.; Hu, L.; Zhang, G.; Yan, T.; Yan, L.; Wei, Q.; Du, B. Removal of Pb(II) and methylene blue from aqueous solution by magnetic hydroxyapatite-immobilized oxidized multi-walled carbon nanotubes. *J. Colloid Interface Sci.* **2017**, *494*, 380–388. [[CrossRef](#)]
15. Wang, Y.; Shi, L.; Gao, L.; Wei, Q.; Cui, L.; Hu, L.; Yan, L.; Du, B. The removal of lead ions from aqueous solution by using magnetic hydroxypropyl chitosan/oxidized multiwalled carbon nanotubes composites. *J. Colloid Interface Sci.* **2015**, *451*, 7–14. [[CrossRef](#)] [[PubMed](#)]
16. Rong, N.; Chen, C.; Ouyang, K.; Zhang, K.; Wang, X.; Xu, Z. Adsorption characteristics of directional cellulose nanofiber/chitosan/montmorillonite aerogel as adsorbent for wastewater treatment. *Sep. Purif. Technol.* **2021**, *274*, 119120. [[CrossRef](#)]
17. Hallam, L.; Papisergio, A.E.; Lessio, M.; Velisek-Carolan, J. Phosphate functionalised titania for heavy metal removal from acidic sulfate solutions. *J. Colloid Interface Sci.* **2021**, *600*, 719–728. [[CrossRef](#)] [[PubMed](#)]
18. Alammari, A.; Park, S.-H.; Ibrahim, I.; Arun, D.; Holtzl, T.; Dumeé, L.F.; Lim, H.N.; Szekely, G. Architecting neonicotinoid-scavenging nanocomposite hydrogels for environmental remediation. *Appl. Mater. Today* **2020**, *21*, 100878. [[CrossRef](#)]
19. Zeng, X.; Yao, H.; Ma, N.; Fan, Y.; Wang, C.; Shi, R. Synthesis, characterization and adsorption performance of a novel post-crosslinked adsorbent. *J. Colloid Interface Sci.* **2011**, *354*, 353–358. [[CrossRef](#)] [[PubMed](#)]
20. Barrejon, M.; Syrgiannis, Z.; Burian, M.; Bosi, S.; Montini, T.; Fornasiero, P.; Amenitsch, H.; Prato, M. Cross-linked carbon nanotube adsorbents for water treatment: Tuning the sorption capacity through chemical functionalization. *ACS Appl. Mater. Interfaces* **2019**, *11*, 12920–12930. [[CrossRef](#)] [[PubMed](#)]
21. Zeng, X.; Yu, T.; Wang, P.; Yuan, R.; Wen, Q.; Fan, Y.; Wang, C.; Shi, R. Preparation and characterization of polar polymeric adsorbents with high surface area for the removal of phenol from water. *J. Hazard. Mater.* **2010**, *177*, 773–780. [[CrossRef](#)] [[PubMed](#)]
22. Zhang, Z.; Jiang, C.; Li, D.; Lei, Y.; Yao, H.; Zhou, G.; Wang, K.; Rao, Y.; Liu, W.; Xu, C.; et al. Micro-mesoporous activated carbon simultaneously possessing large surface area and ultra-high pore volume for efficiently adsorbing various VOCs. *Carbon* **2020**, *170*, 567–579. [[CrossRef](#)]
23. Zhao, D.; Huo, Q.; Feng, J.; Chmelka, B.F.; Stucky, G.D. Nonionic triblock and star diblock copolymer and oligomeric surfactant syntheses of highly ordered, hydrothermally stable, mesoporous silica structures. *J. Am. Chem. Soc.* **1998**, *120*, 10546. [[CrossRef](#)]
24. Zhao, D.; Feng, J.; Huo, Q.; Melosh, N.; Fredrickson, G.H.; Chmelka, B.F.; Stucky, G.D. Triblock copolymer syntheses of mesoporous silica with periodic 50 to 300 angstrom pores. *Science* **1998**, *279*, 548–552. [[CrossRef](#)] [[PubMed](#)]
25. Liu, C.; Kubo, T.; Naito, T.; Otsuka, K. Controllable molecular sieving by copoly(poly(ethylene glycol) acrylate/poly(ethylene glycol) diacrylate)-based hydrogels via capillary electrophoresis for DNA fragments. *ACS Appl. Polym. Mater.* **2020**, *2*, 3886–3893. [[CrossRef](#)]
26. Hardian, R.; Pogany, P.; Lee, Y.M.; Szekely, G. Molecular sieving using metal-polymer coordination membranes in organic media. *J. Mater. Chem. A* **2021**, *9*, 14400–14410. [[CrossRef](#)]
27. Gong, T.; Li, Y.; Zhang, H.; Zhou, J.; Xie, G.; Lei, B.; Zhuang, J.; Liu, Y.; Zhang, H. Synthesis of SBA-15 assembled with silicon nanoparticles with different morphologies for oxygen sensing. *Microporous Mesoporous Mater.* **2020**, *296*, 110001. [[CrossRef](#)]
28. Gonzalez-Rodriguez, J.; Fernandez, L.; Vargas-Osorio, Z.; Vazquez-Vazquez, C.; Pineiro, Y.; Rivas, J.; Feijoo, G.; Moreira, M.T. Reusable Fe<sub>3</sub>O<sub>4</sub>/SBA15 nanocomposite as an efficient photo-fenton catalyst for the removal of sulfamethoxazole and orange II. *Nanomaterials* **2021**, *11*, 533. [[CrossRef](#)]
29. Han, J.; Fang, P.; Jiang, W.; Li, L.; Guo, R. Ag-nanoparticle-loaded mesoporous silica: Spontaneous formation of Ag nanoparticles and mesoporous silica SBA-15 by a one-pot strategy and their catalytic applications. *Langmuir* **2012**, *28*, 4768–4775. [[CrossRef](#)] [[PubMed](#)]
30. Liu, H.; Ding, W.; Lei, S.; Tian, X.; Zhou, F. Selective adsorption of CH<sub>4</sub>/N<sub>2</sub> on Ni-based MOF/SBA-15 composite materials. *Nanomaterials* **2019**, *9*, 149. [[CrossRef](#)]
31. Cheng, M.; Wang, Z.; Lv, Q.; Li, C.; Sun, S.; Hu, S. Preparation of amino-functionalized Fe<sub>3</sub>O<sub>4</sub>@mSiO<sub>2</sub> core-shell magnetic nanoparticles and their application for aqueous Fe<sup>3+</sup> removal. *J. Hazard. Mater.* **2018**, *341*, 198–206.
32. Sierra, I.; Perez-Quintanilla, D. Heavy metal complexation on hybrid mesoporous silicas: An approach to analytical applications. *Chem. Soc. Rev.* **2013**, *42*, 3792–3807. [[CrossRef](#)]
33. Kisszekelyi, P.; Hardian, R.; Vovusha, H.; Chen, B.; Zeng, X.; Schwingenschlogl, U.; Kupai, J.; Szekely, G. Selective electrocatalytic oxidation of biomass-derived 5-hydroxymethylfurfural to 2,5-diformylfuran: From mechanistic investigations to catalyst recovery. *ChemSusChem* **2020**, *13*, 3127–3136. [[CrossRef](#)] [[PubMed](#)]

34. Mahmoudi, B.; Rostami, A.; Kazemnejadi, M.; Hamah-Ameen, B.A. Catalytic oxidation of alcohols and alkyl benzenes to carbonyls using  $\text{Fe}_3\text{O}_4@\text{SiO}_2@(\text{TEMPO})\text{-co-(Chlorophyll-Co}^{\text{III}})$  as a bi-functional, self-co-oxidant nanocatalyst. *Green Chem.* **2020**, *22*, 6600–6613. [[CrossRef](#)]
35. Permien, S.; Indris, S.; Schurmann, U.; Kienle, L.; Zander, S.; Doyle, S.; Bensch, W. What happens structurally and electronically during the Li conversion reaction of  $\text{CoFe}_2\text{O}_4$  nanoparticles: An operando XAS and XRD investigation. *Chem. Mater.* **2016**, *28*, 434–444. [[CrossRef](#)]
36. Liu, T.; Han, X.; Wang, Y.; Yan, L.; Du, B.; Wei, Q.; Wei, D. Magnetic chitosan/anaerobic granular sludge composite: Synthesis, characterization and application in heavy metal ions removal. *J. Colloid Interface Sci.* **2017**, *508*, 405–414. [[CrossRef](#)] [[PubMed](#)]
37. Azizian, S.; Haerifar, M.; Bashiri, H. Adsorption of methyl violet onto granular activated carbon: Equilibrium, kinetics and modeling. *Chem. Eng. J.* **2009**, *146*, 36–41. [[CrossRef](#)]
38. Yu, X.-Y.; Luo, T.; Zhang, Y.-X.; Jia, Y.; Zhu, B.-J.; Fu, X.-C.; Liu, J.-H.; Huang, X.-J. Adsorption of lead(II) on  $\text{O}_2$ -plasma-oxidized multiwalled carbon nanotubes: Thermodynamics, kinetics, and desorption. *ACS Appl. Mater. Interfaces* **2011**, *3*, 2585–2593. [[CrossRef](#)] [[PubMed](#)]
39. Jain, S.N.; Shaikh, Z.; Mane, V.S.; Vishnoi, S.; Mawal, V.N.; Patel, O.R.; Bhandari, P.S.; Gaikwad, M.S. Nonlinear regression approach for acid dye remediation using activated adsorbent: Kinetic, isotherm, thermodynamic and reusability studies. *Microchem. J.* **2019**, *148*, 605–615. [[CrossRef](#)]